Applied Catalysis B: Environmental 88 (2009) 142–151

Contents lists available at ScienceDirect

Applied Catalysis B: Environmental

journal homepage: www.elsevier.com/locate/apcatb

Simultaneous production of hydrogen and multi-walled carbon nanotubes by ethanol decomposition over Ni/Al_2O_3 catalysts

Gang Wang [a], Hui Wang [a,*], Zongxun Tang [a], Weilong Li [a,b], Jinbo Bai [c]

[a] Key Laboratory of Synthetic and Natural Functional Molecule Chemistry (Ministry of Education), Department of Chemistry, Northwest University, Xi'an 710069, PR China
[b] Institute of Photonics & Photon-Technology, Northwest University, Xi'an 710069, PR China
[c] Lab. MSS/MAT, CNRS UMR 8579, Ecole Centrale Paris, 92295 Chatenay Malabry, France

ARTICLE INFO

Article history:
Received 21 July 2008
Received in revised form 15 September 2008
Accepted 15 September 2008
Available online 21 September 2008

Keywords:
Ethanol decomposition
Ni/Al_2O_3
Hydrogen
Carbon nanotubes
Carbon nanofibers

ABSTRACT

Ethanol decomposition was studied over Ni/Al_2O_3 catalysts with different Ni loadings (10–90 mol%) at temperatures between 500 and 800 °C to produce hydrogen and multi-walled carbon nanotubes (MWCNTs) at the same time. The hydrogen production increased with increasing temperature and Ni loadings. However, both the quality and the quantity of the nanotubes formed at the relatively high temperatures of 700 and 800 °C decreased due to sintering of the Ni particles. The Ni (80 mol%)/Al_2O_3 was the most effective catalyst for ethanol decomposition into hydrogen (the maximum H_2 yield of 83%) and MWCNTs (the maximum deposited yield of 80%) at 600 °C. Carbon nanofibers (CNFs) and MWCNTs were observed simultaneously on Ni (90 mol%)/Al_2O_3 at 500 °C. Several possible reactions also were proposed to explain ethanol decomposition to produce hydrogen and carbon (including nanotube), etc., at the same time.

1. Introduction

Hydrogen is an attractive power source because of its high conversion efficiency and low pollutant emissions [1]. There are four traditional methods for hydrogen production at present: water electrolysis, gasification reactions, partial oxidation reactions of heavy oil, and hydrocarbon steam reforming reactions [2,3]. Recently, a method of hydrogen production by the decomposition of methane attracts great attention. In addition to the production of hydrogen, it also results in the generation of nanocarbon materials like carbon nanofibers (CNFs) or carbon nanotubes (CNTs) [4–9]. However, methane mainly comes from natural gas, which is a non-renewable resource. From an environmental point of view ethanol is an appropriate candidate for hydrogen production via steam reform, photo-catalysis and decomposition [3,10–13], because it could be considered a renewable raw material that can be easily obtained from biomass. Several research groups reported the production of hydrogen via ethanol decomposition under different conditions [14–16], but none of them mentioned the production of CNFs or CNTs accompanied by hydrogen during ethanol decomposition.

CNTs have been paid increasing attention due to their extraordinary mechanical, electric, and thermal properties [17]. Therefore, the synthesis of higher quality CNTs at lower cost is of great importance. Compared with the laser ablation [18] and arc-discharge [19], the chemical vapor deposition (CVD) [20] has been dominant for the mass production of CNTs. It has been reported that single-walled carbon nanotubes (SWCNTs) [21–23], multi-walled carbon nanotubes (MWCNTs) [24,25] and carbon nanotube fibers [26] were successfully synthesized by CVD using ethanol as carbon source decomposition over various catalysts. However, the hydrogen production has not been involved in these reported papers, i.e. the amount of hydrogen produced from the ethanol decomposition has not been systematically investigated yet.

Although the decomposition of methane into hydrogen and CNTs has been widely described [4–6], fewer studies have dealt with the production of hydrogen and CNTs by ethanol decomposition [27]. Recently, we have studied systemically the catalytic activities of supported Fe catalysts for the co-production of hydrogen and CNTs from the decomposition of ethanol. The results indicated that Fe/Al_2O_3 was a quite active catalyst for the co-production of hydrogen and CNTs and that its activity and stability depended strongly on the Fe loading [28]. It is well known that supported Ni metal catalyst is one of the effective catalysts for the decomposition of hydrocarbons. Literature reports have also showed that Ni catalyst favors the decomposition of ethanol to synthesize CNTs [29]. In the present work, we choose Ni metal as catalyst and investigate the catalytic performance of Ni catalysts supported on Al_2O_3 for the decomposition of ethanol to produce hydrogen and CNTs in the range of temperature between 500 and

* Corresponding author. Tel.: +86 29 8836 3115; fax: +86 29 8830 3798.
E-mail address: huiwang@nwu.edu.cn (H. Wang).

0926-3373/$ – see front matter © 2008 Elsevier B.V. All rights reserved.
doi:10.1016/j.apcatb.2008.09.008

800 °C. The effect of the temperature and the Ni loadings on the production of hydrogen and MWCNTs will also be discussed. Al_2O_3 was chosen as support because it ensures thermal stability of the catalyst [10]. For comparison, the decomposition reaction of ethanol in the absence of Ni catalyst or Al_2O_3 support was also carried out under the same experimental conditions. Therefore, the aim of the present work was to determine an optimum experimental condition for a maximum yield of hydrogen production and MWCNT growth by bioethanol decomposition, which may have important technological application.

2. Experimental

2.1. Preparation of catalysts

Ni/Al_2O_3 catalysts with different loading amounts of Ni were prepared using a hydrothermal method. The loading amount of Ni in the Ni/Al_2O_3 catalysts was adjusted to *x* mol% of total metal (Ni and Al) cations (10 mol% means Ni/(Ni + Al) = 10%) and varied from 10 to 90 mol% at 10 intervals. The detailed procedure of the catalyst preparation is as follows: an aqueous solution of 10 ml containing predetermined amounts of $Ni(NO_3)_2{\cdot}6H_2O$ and $Al(NO_3)_3{\cdot}9H_2O$ was first prepared. The pH value of the solution was adjusted to 8 by adding $NH_3{\cdot}H_2O$ solution of 25 wt% gradually with constant stirring to obtain the catalysts with different loadings of Ni. The mixture was aged at room temperature for 4 h. Thus, a binary colloid was achieved. The colloid was placed in a 25 ml capacity Teflon-lined stainless steel autoclave. It was heated at 140 °C for 48 h. The hydrothermal products were collected by sedimentation and washed with deionized water 5 times, followed by drying at 80 °C for 12 h and calcining at 350 °C for 5 h, and subsequently at 500 °C for 10 h in air. The prepared catalysts or catalyst precursors were denoted as Ni (*X* mol%)/Al_2O_3, where *X* mol% is the mol% loading in terms of Ni. The prepared sample in the absence of catalyst or support is denoted as the blank Al_2O_3 or the Ni sample.

2.2. Ethanol decomposition

The reaction apparatus used for ethanol decomposition was a conventional gas flow system with a vertical fixed bed at the center of a quartz tubular reactor (inner diameter 5 mm). The temperature of the bed was monitored with a thermocouple touched to the outside wall of the reactor in close proximity to the catalyst disc. Prior to ethanol decomposition, the catalyst (150 mg) was reduced by hydrogen at 500 °C for 1 h and purged under Ar at the same temperature for 30 min. Then the decomposition of ethanol was performed on the Ni/Al_2O_3 catalysts at the temperatures of 500, 600, 700 and 800 °C. Ethanol was injected through a microinjector into a vaporizing chamber (100 °C) at a flow rate of 0.3 ml/h and switched to the tubular reactor using Ar (40 ml/min) as the carrier gas. During ethanol decomposition, the gaseous products in the exit gas from the tubular reactor were analyzed at 6 min intervals by a gas chromatography (GC). After 50 min, the ethanol feed was stopped. The solid products were collected from the tubular reactor.

2.3. Characterization

The scanning electron micrography (SEM) images and back-scattering electron images (BEI) of the catalysts with solid products by ethanol decomposition were measured using a FEI Quanta 400 ESEM-FEG (environmental scanning electron microscope-field emission gun) at an accelerating voltage of 15 kV. The transmission electron microscope (TEM) images of MWCNTs were recorded with a JEOL JEM-3010 high-resolution transmission electron microscope (HRTEM) at an accelerating voltage of 300 kV. Raman scattering analysis was performed by a dispersive Raman spectrometer (Nicolet, ALMEGA) with the excitation wavelength of 532 nm. X-ray diffraction (XRD, D/max-3c, Cu Kα, 50 kV, 300 mA, at room temperature in air) was used to characterize the compositions of the catalyst after reduction with hydrogen at 500 °C and of the catalyst with solid products after ethanol decomposition.

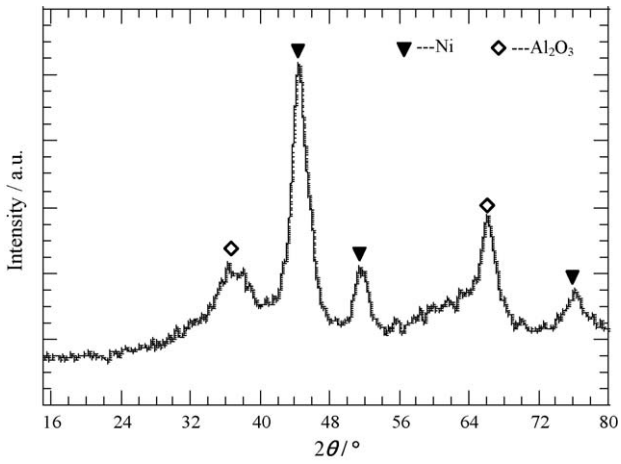

Fig. 1. XRD pattern of the reduced Ni (30 mol%)/Al_2O_3 catalyst at 500 °C.

Fig. 1 shows the XRD pattern of the reduced Ni(30 mol%)/Al_2O_3 catalyst. It is obvious that only the peaks due to Ni metal and Al_2O_3 can be observed in the XRD pattern, indicating that the catalyst has been reduced at 500 °C.

2.4. Evaluation of catalytic performance of Ni/Al_2O_3 catalysts

The process efficiency was evaluated in terms of ethanol conversion, the yields of H_2 and the deposited carbon. Ethanol conversion and H_2 yield were calculated according to the following Eqs. (1′) and (2′), respectively. The deposited carbon yield was calculated as the amount of carbon formed relatively to the total amount of carbon fed into the reactor as shown in Eq. (3′).

$$\text{Ethanol conversion}(\%) = \frac{\text{mol (ethanol) in} - \text{mol (ethanol) out}}{\text{mol (ethanol) in}} \times 100 \quad (1')$$

$$\text{H}_2\text{ yield }(\%) = \frac{\text{mol of hydrogen atom converted to H}_2}{\text{mol of hydrogen atom contained in the feed}} \times 100 \quad (2')$$

$$\text{Deposited carbon yield}(\%) = \frac{\text{C deposited}}{\text{C available}} \times 100 \quad (3')$$

3. Results and discussion

3.1. Ethanol conversion

Catalytic reactions of ethanol decomposition were carried out in a temperature range of 500–800 °C over Ni/Al_2O_3 catalysts with a loading amount of Ni in the range of 10–90 mol%. Fig. 2 shows the changes of ethanol conversion as a function of temperature for ethanol decomposition. It is found that ethanol conversion depended strongly on the Ni loading amount and the reaction temperature, and basically increased with the increase of Ni loadings and temperatures. Although the higher temperatures favored the decomposition of ethanol, ethanol conversion did not

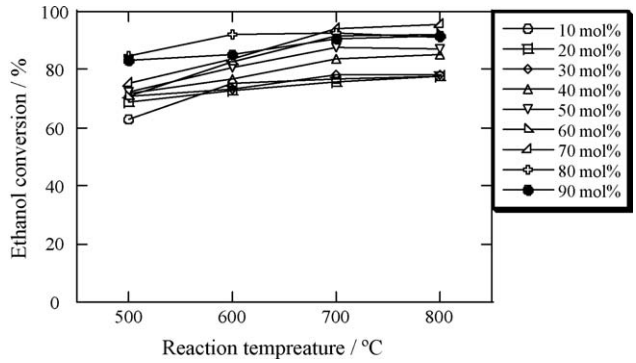

Fig. 2. Changes of ethanol conversion as a function of the reaction temperature in ethanol decomposition over Ni/Al_2O_3 catalysts with different metal loadings, the feeding rate of ethanol = 0.3 ml/h, the flow rate of carrier gas = 40 ml/min.

show obvious increment for the various Ni loading catalysts in the range of 700–800 °C, especially for those catalysts with a relatively higher loading of Ni (≥50 mol%). For example, for the Ni(80 mol%)/Al_2O_3 catalyst, as the temperature increased from 500 to 600 °C the ethanol conversion obviously increased from 84.2 to 92.8%, showing around a increment of 9%; when the temperatures increased from 700 to 800 °C, almost a zero increment from 93.6 to 93.8% was observed in Fig. 2. We can conclude that a favorable temperature of ethanol decomposition was in the range of 600–700 °C. If the energy consumption was considered, 600 °C was regarded as an optimum temperature for ethanol decomposition.

3.2. H_2 produced from ethanol decomposition

Fig. 3 shows the changes of H_2 yield as a function of the reaction time for ethanol decomposition over Ni/Al_2O_3 catalysts at the temperatures of 500, 600, 700 and 800 °C. The Ni loadings in Ni/Al_2O_3 catalysts varied from 10 to 90 mol% at 10 intervals. The kinetic curve of the H_2 yield with time either in the absence of catalyst (no loading) or in the absence of support (no support) is also inserted in Fig. 3 for comparison.

3.2.1. Effect of Ni catalyst on H_2 yield

As can be seen in Fig. 3(a)–(d), the H_2 yield in the absence of catalyst (0 mol% or blank Al_2O_3 sample) was rather low, nearly being zero at 500 and 600 °C and not more than 35% at 700 and 800 °C, so ethanol decomposition over Al_2O_3 support was negligible at lower temperatures. However, the H_2 yield in the absence of support (100 mol% or Ni sample) remained an almost constant (~50 to 60%) for the decomposition of ethanol at any temperature, showing the efficiency of Ni metal as catalyst for hydrogen production and the necessity of Al_2O_3 presence as dispersant in the catalyst.

3.2.2. Effect of Ni loading and temperature on H_2 yield

It is found that altering the amount of Ni loadings in Ni/Al_2O_3 catalysts and the reaction temperature could control the H_2 yield. It is apparent from Fig. 3(a) that the H_2 yield increased slightly (40–60%) as the Ni loadings rising from 10 to 90 mol% at 500 °C. A relatively great increase in the H_2 yield was observed in Fig. 3(b) when the temperature reached to 600 °C, showing the catalysts higher catalytic activities at 600 °C than those at 500 °C. As the temperature increased to 700 °C, the effect of Ni loadings on the H_2 yield became more apparent. However, the changes of the H_2 yield in Fig. 3(d) were obviously different from those in Fig. 3(a)–(c). It is found that the Ni/Al_2O_3 catalysts with lower Ni loadings (10–40 mol%) displayed a much lower catalytic activity than those with higher loadings (50–90 mol%) at 800 °C, and even

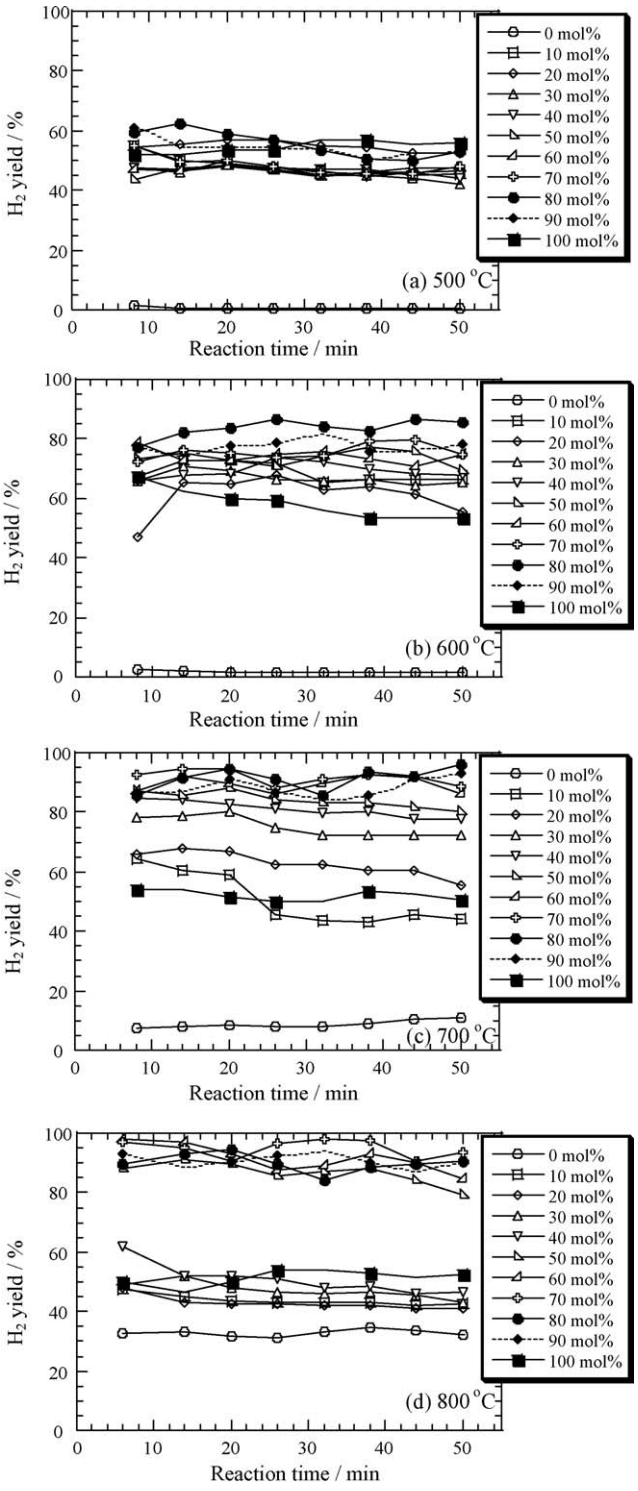

Fig. 3. Changes of H_2 yield as a function of the reaction time in ethanol decomposition over Ni/Al_2O_3 catalysts with different Ni loadings at different temperatures: (a) 500, (b) 600, (c) 700, and (d) 800 °C. For comparison, the results in the absence of catalyst or support are inserted.

lower than the same Ni loading catalysts at 600 or 700 °C. The results indicate that the Ni/Al_2O_3 catalysts with lower Ni loadings (≤40 mol%) at a high temperature of 800 °C did not effectively enhance H_2 yield but did effectively at a relatively lower temperature of 600 or 700 °C, while for those with relatively higher Ni loadings the H_2 yield could be effectively increased with increasing temperature from 500 to 800 °C.

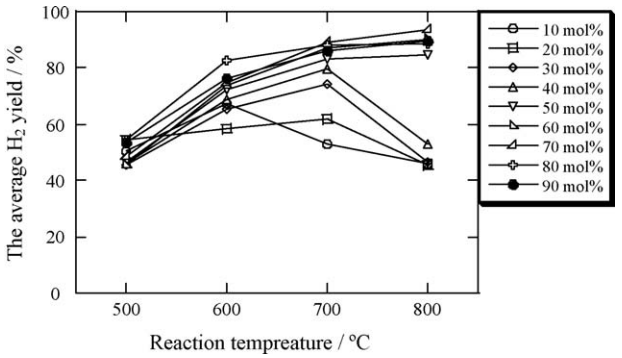

Fig. 4. Changes of the average H_2 yield vs. temperature for ethanol decomposition over Ni/Al_2O_3 catalysts at the temperatures of 500, 600, 700 and 800 °C.

In order to gain further insight into the results mentioned above, Fig. 4 shows the changes of the average H_2 yield vs. temperature for ethanol decomposition over Ni/Al_2O_3 catalysts with the Ni loadings of 10–90 mol%. It is obvious that the Ni/Al_2O_3 catalysts can be divided into two groups based on the features of kinetic curves: (1) the catalysts with a relatively higher loading of Ni (≥50 mol%) and (2) those with a relatively lower loading of Ni (≤40 mol%). For the catalysts with the higher Ni loadings, the average H_2 yield gradually increased with temperature, reaching ~80–90% at 700 °C and ~80–95% at 800 °C; the average H_2 yield for the Ni (70 mol%)/Al_2O_3 catalyst exhibited a maximum (~95%) at 800 °C and for the Ni (60, 80 and 90 mol%)/Al_2O_3 catalysts reached a constant value, 90%, at 800 °C. For the catalysts with the lower Ni loadings, the average H_2 yield firstly increased with the temperature increased from 500 to 700 °C and subsequently decreased at 800 °C. It concluded that rising temperature favored the increase of H_2 yield for the higher Ni loading catalysts, however, a high temperature of 800 °C would result in the decrease of H_2 yield for those with the lower Ni loadings. We assume that it may be related to the effective action of the active phase (Ni) in the Ni/Al_2O_3 catalysts on hydrogen production. For the lower Ni loading catalysts, the amount of active phase might be reduced due to the sintering of Ni metal at a relatively higher temperature of 800 °C. As a result, the H_2 yield obtained over the catalysts could be obviously decreased. While for the higher Ni loading catalysts, the H_2 yield at 800 °C was expected to decrease because the Ni particle also was sintered similarly. However, the H_2 yield did not obviously decrease as expectation, and in contrast, the H_2 yield increased slightly. The reason may be relevant to the fact that the mole fraction of Ni in the higher loading catalysts was too high to decrease the amount of active phase more obviously than do that in the lower loading catalysts at 800 °C.

Laosiripojana et al. [15] reported the maximum yield of 60% for the ethanol decomposition over CeO_2 catalysts and of 55% for Ni/Al_2O_3 catalysts in the temperature range of 700–1000 °C. Barthos et al. [16] indicated the H_2 yield of 70% for the ethanol decomposition over Mo_2C/carbon catalysts. Our experimental results showed that the maximum H_2 yield for the Ni (80 mol%)/Al_2O_3 catalyst at 600 °C reached 83% and for the Ni (60–90 mol%)/Al_2O_3 catalysts at 700 °C attained around 90%, any of which was much greater than reported data.

3.3. Catalyst activity and lifetime for hydrogen production

As catalyst for hydrogen production, the catalyst lifetime is an important issue, and any deposited carbon accompanied with hydrogen production on the surface of catalysts (including nanotube growth) will deactivate catalyst. If just considering hydrogen generation, it is necessary to investigate the catalyst activity and lifetime. Fig. 5 shows the H_2 yield versus time in ethanol decomposition over the Ni(30 and 80 mol%)/Al_2O_3 catalysts at two different temperatures (600 and 700 °C). Ethanol decomposition was performed until the catalyst deactivation in the maximum time delay of 100 h. It is obvious that the Ni loading and reaction temperature affected the catalyst lifetime and activity.

The Ni(30 mol%)/Al_2O_3 catalyst was found to show a relatively higher catalytic activity with a shorter term stability at initial stage at 700 °C than that at 600 °C. At 700 °C a maximum H_2 yield of about 78% in the range of only 0–0.25 h was obtained and subsequent it quickly decreased from 78 to 42% in the range of also only 0.25–3 h and kept the yield of about 42% for around 30 h until the complete deactivation of the catalyst after 53 h. While at 600 °C an almost constant H_2 yield of about 65% in the range of 0–13.5 h was maintained and subsequent it decreased gradually until complete deactivation of Ni (30 mol%)/Al_2O_3 after 65 h. The above results indicated that higher temperature could enhance the initial activity of the catalyst but also cause rapidly deactivation, i.e., the decrease of the catalyst lifetime. A possible explanation for it may be due to the formation of a high yield of amorphous carbon on the catalyst at a relatively high temperature of 700 °C, which may encapsulate the metallic particles and prevent ethanol from reaching the catalyst or poison the active metal sites.

The Ni(80 mol%)/Al_2O_3 catalyst at 600 °C showed a relatively higher activity and longer stability than Ni(30 mol%)/Al_2O_3 due to no obvious deactivation at initial 5 h and a slight deactivation in the range of 5–14 h. A maximum H_2 yield of about 80% in the range of 0–2 h and the H_2 yield of higher than 67% in the range of 2–14 h were obtained, respectively. An almost constant H_2 yield of about

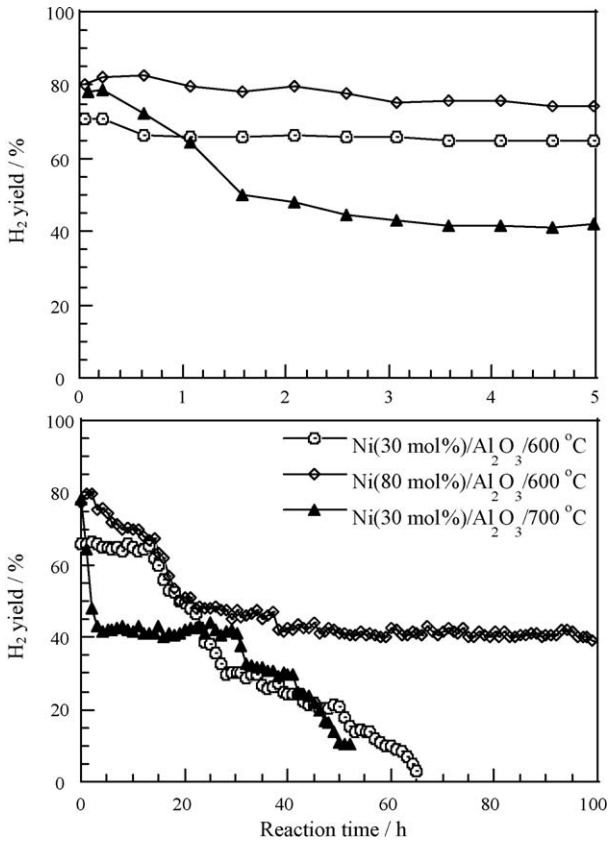

Fig. 5. Changes of H_2 yield as a function of the reaction time in ethanol decomposition over the Ni (30 and 80 mol%)/Al_2O_3 catalysts at the reaction conditions shown.

42% in the maximum time delay range of 38–100 h also showed that the Ni(80 mol%)/Al_2O_3 catalyst had a much longer catalytic life than that of Ni(30 mol%)/Al_2O_3 at 600 °C for hydrogen production. A possible reason is that a relatively high number of the active metal site is responsible for enhancing performance of the catalyst. This also is the reason why ethanol decomposed over Ni(80 mol%)/Al_2O_3 could produce a high yield of hydrogen at 600 °C, as described previously. In terms of just considering hydrogen production, it is concluded that the Ni(80 mol%)/Al_2O_3 catalyst had a relatively higher activity and longer lifetime than the Ni(30 mol%)/Al_2O_3 catalyst at 600 °C.

3.4. MWCNTs synthesized from ethanol decomposition

3.4.1. Influence of temperature on MWCNT growth

Fig. 6 shows SEM images of MWCNTs formed by ethanol decomposition over the Ni (30 mol%)/Al_2O_3 catalyst at 500, 600, 700 and 800 °C. The SEM images in Fig. 6(a) and (b) indicate the formation of dense MWCNTs with few metal particles and a little amorphous carbon on the catalyst at 500 and 600 °C. However, the amount of MWCNTs on the catalyst decreased quickly as the temperature was increased to 700 or 800 °C. It is evident from Fig. 6(c) and (d) that a few of MWCNTs with a wide diameter distribution (40–80 nm) was observed on the catalyst at 700 or 800 °C, and more impurity such as metal particles and amorphous carbon appeared and aggregated together with the MWCNTs. It shows that the Ni (30 mol%)/Al_2O_3 catalyst at lower temperatures (500 and 600 °C) was more effective for ethanol decomposition to produce MWCNTs than that at higher temperatures (700 and 800 °C). Perhaps the decrease in the density of MWCNTs at elevated temperatures is closely correlated with a decrease in the amount of smaller Ni particles on the surface of catalyst due to the serious sintering of Ni metal particles [30]. In addition, XRD pattern of MWCNTs grown over the Ni (30 mol%)/Al_2O_3 catalyst at 600 °C in Fig. 7 also indicates the presence of Ni particles in the final products besides MWCNTs.

The effects of temperature on the MWCNT growth were further investigated with Raman analysis. Fig. 8 illustrates the Raman spectra of MWCNTs formed by ethanol decomposition over the Ni (30 mol%)/Al_2O_3 catalyst at 500, 600, 700 and 800 °C. For all the Raman spectra, two bands were observed at ca. 1590 (G band) and 1350 cm^{-1} (D band). The G band corresponds to the in-plane oscillation of carbon atoms in the sp^2 graphite sheet of CNTs, indicating ordered structures in the CNTs. The D band represents the structural imperfection of graphite sheet [31], indicating defects and impurity in the CNTs. Generally, the structure of CNTs can be evaluated by the I_G/I_D ratio between the intensities of G and D bands. A larger I_G/I_D ratio means a relatively perfect structure and purity for the CNTs [32]. Fig. 8 shows that the I_G/I_D ratio of the samples increased in the temperature order of 800 °C

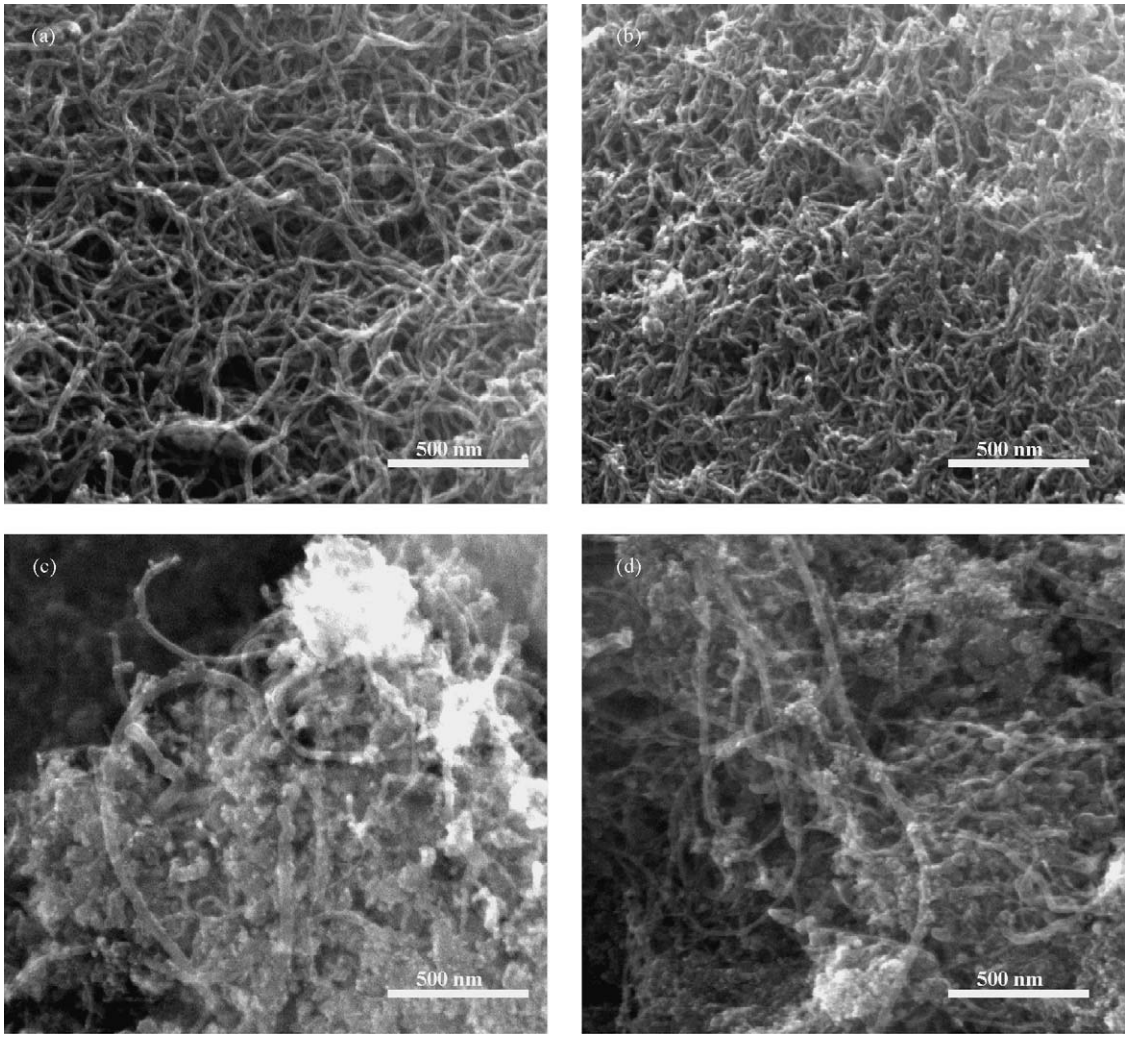

Fig. 6. SEM images of MWCNTs formed by ethanol decomposition over Ni (30 mol%)/Al_2O_3 catalyst at different temperatures: (a) 500, (b) 600, (c) 700, and (d) 800 °C.

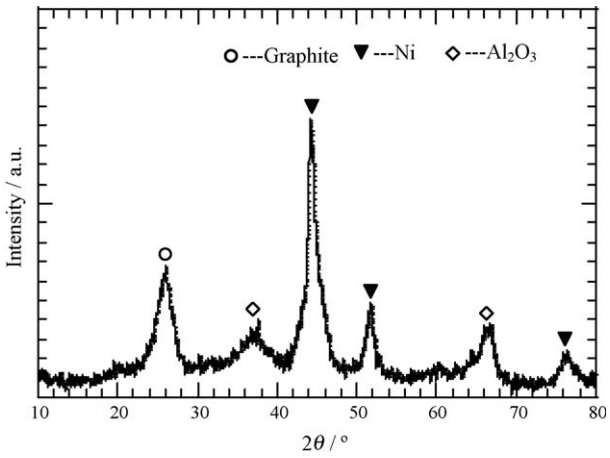

Fig. 7. XRD pattern of MWCNTs grown on the Ni(30% mol)/Al_2O_3 catalyst at 600 °C.

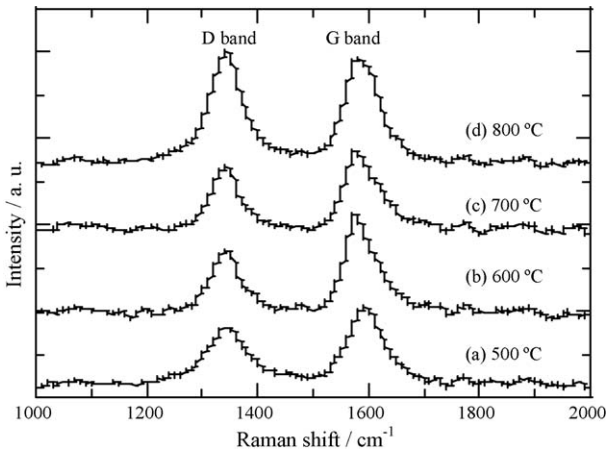

Fig. 8. Raman spectra of MWCNTs formed by ethanol decomposition over Ni (30 mol%)/Al_2O_3 catalyst at different temperatures: (a) 500, (b) 600, (c) 700, and (d) 800 °C.

(I_G/I_D = 0.9) < 700 °C (I_G/I_D = 1.0) < 500 °C (I_G/I_D = 1.3) < 600 °C (I_G/I_D = 1.5). The result indicates that MWCNTs grown at 600 °C were of relatively higher purity and lower defects inside the graphite sheet than those grown at other temperatures. In other words, the decomposition of ethanol over the Ni (30 mol%)/Al_2O_3 catalyst at 600 °C was more suitable for obtaining MWCNTs both in quantity and in quality.

Figs. 9 and 10 show TEM images of MWCNTs grown by ethanol decomposition over the Ni (30 mol%)/Al_2O_3 catalyst at 500 and 600 °C (reaction time: 50 min, the feeding rate of ethanol: 0.3 ml/h, the flow rate of carrier gas: 40 ml/min), respectively. The crooked nanotubes with a broader diameter distribution were observed in Fig. 9(a) at 500 °C. The outer diameters of MWCNTs grown at this temperature varied from 10 to 30 nm, and the inner diameters were about 3–5 nm. The higher magnification TEM image in Fig. 9(b) shows that the graphitic sheets were not parallel to the tube axis (about 45°), and MWCNTs appeared to be a fish-bone type in the cross-section. The structure was similar to that reported by several other research groups [9,33,34]. For MWCNTs grown on the Ni (30 mol%)/Al_2O_3 catalyst at 600 °C, the diameter showed a distribution from 8 to 10 nm (Fig. 10(a)). The higher magnification TEM image in Fig. 10(b) shows that the outer and the inner diameters of MWCNTs were about 10 and 3 nm, respectively. The graphitic sheets in the walls formed at 600 °C were more parallel to the tube axis than those formed at 500 °C, and the fringes of the walls for MWCNTs at 600 °C were relatively more perfect than those at 500 °C. This is in agreement with the above-mentioned results by Raman spectra analysis. It also further indicates that the Ni (30 mol%)/Al_2O_3 catalyst at 600 °C could accelerate ethanol decomposition effectively to grow relatively high-quality MWCNTs compared with that at other temperatures.

3.4.2. *Influence of Ni loadings on MWCNT growth*

The SEM images of MWCNTs formed at 600 °C by ethanol decomposition over Ni/Al_2O_3 catalysts with four different Ni loadings (50, 70, 80 and 90 mol%) are showed in Fig. 11(a)–(d). All the SEM images showed the presence of CNTs, which consisted of highly entangled, cross-linked and web-like MWCNTs. No obvious differences in the density and diameter of MWCNTs were observed in Fig. 11(a)–(d) for these catalysts with different Ni loadings, suggesting that the size of Ni metal particle at 600 °C with increasing Ni loading might change not a lot (or slightly).

Fig. 12 shows that the deposited carbon yield varied with the Ni loadings in ethanol decomposition over Ni/Al_2O_3 catalysts at 600 °C. The reaction condition in Fig. 12 was similar to that in Fig. 10. It is seen that the deposited carbon yield varied between 60 and 80%. The yield decreased slightly as the Ni loadings increased

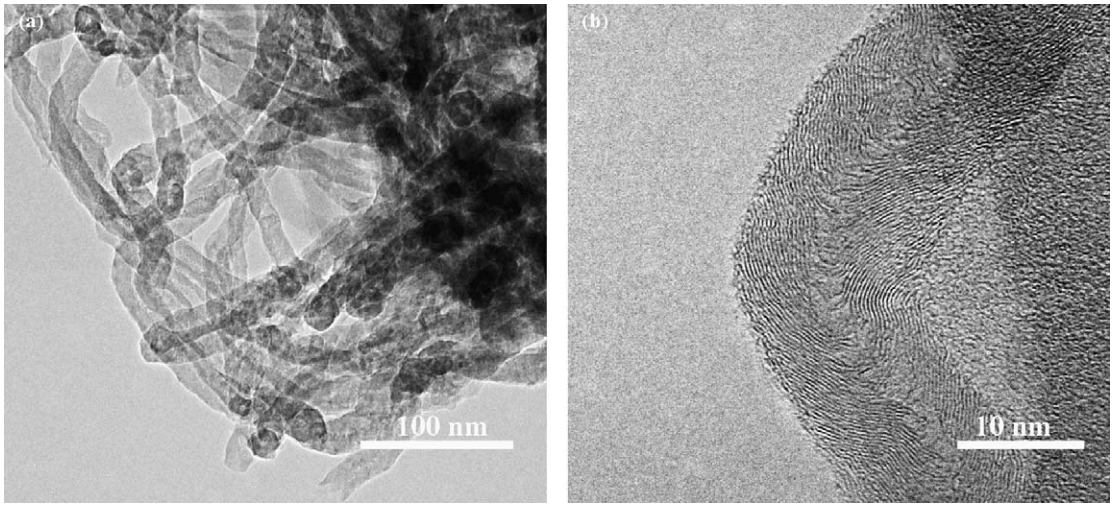

Fig. 9. TEM images of MWCNTs formed by ethanol decomposition over Ni (30 mol%)/Al_2O_3 catalyst at 500 °C.

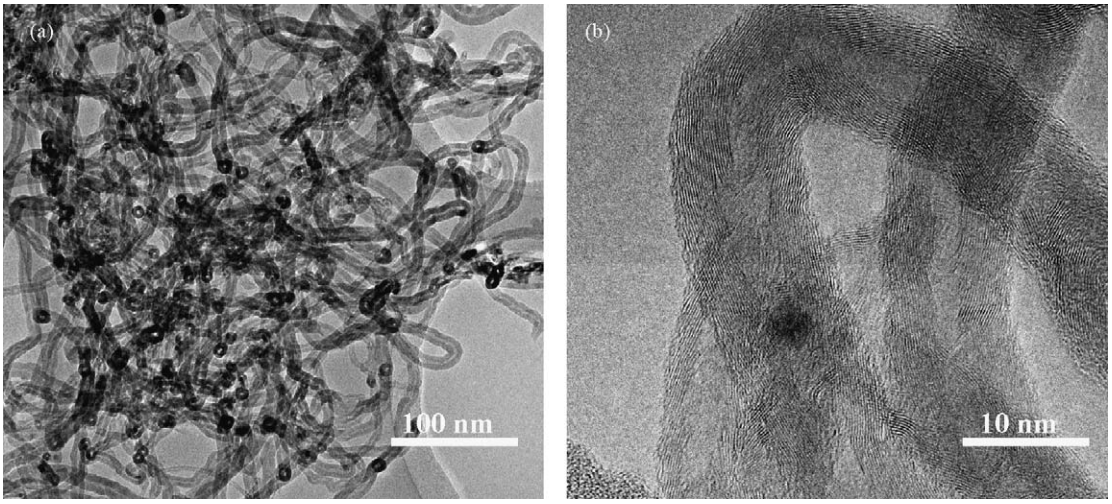

Fig. 10. TEM images of MWCNTs formed by ethanol decomposition over Ni (30 mol%)/Al_2O_3 catalyst at 600 °C.

from 10 to 20 mol%, then increased gradually with the Ni loadings and reached a maximum value (80%) for the Ni (80 mol%)/Al_2O_3 catalyst. At this moment, any further increase in the Ni loadings would result in the reduction of the deposited carbon yield.

3.5. Formation of CNFs and MWCNTs

It is interesting that two types of carbon deposits with different morphologies (CNFs and MWCNTs) were observed by SEM after

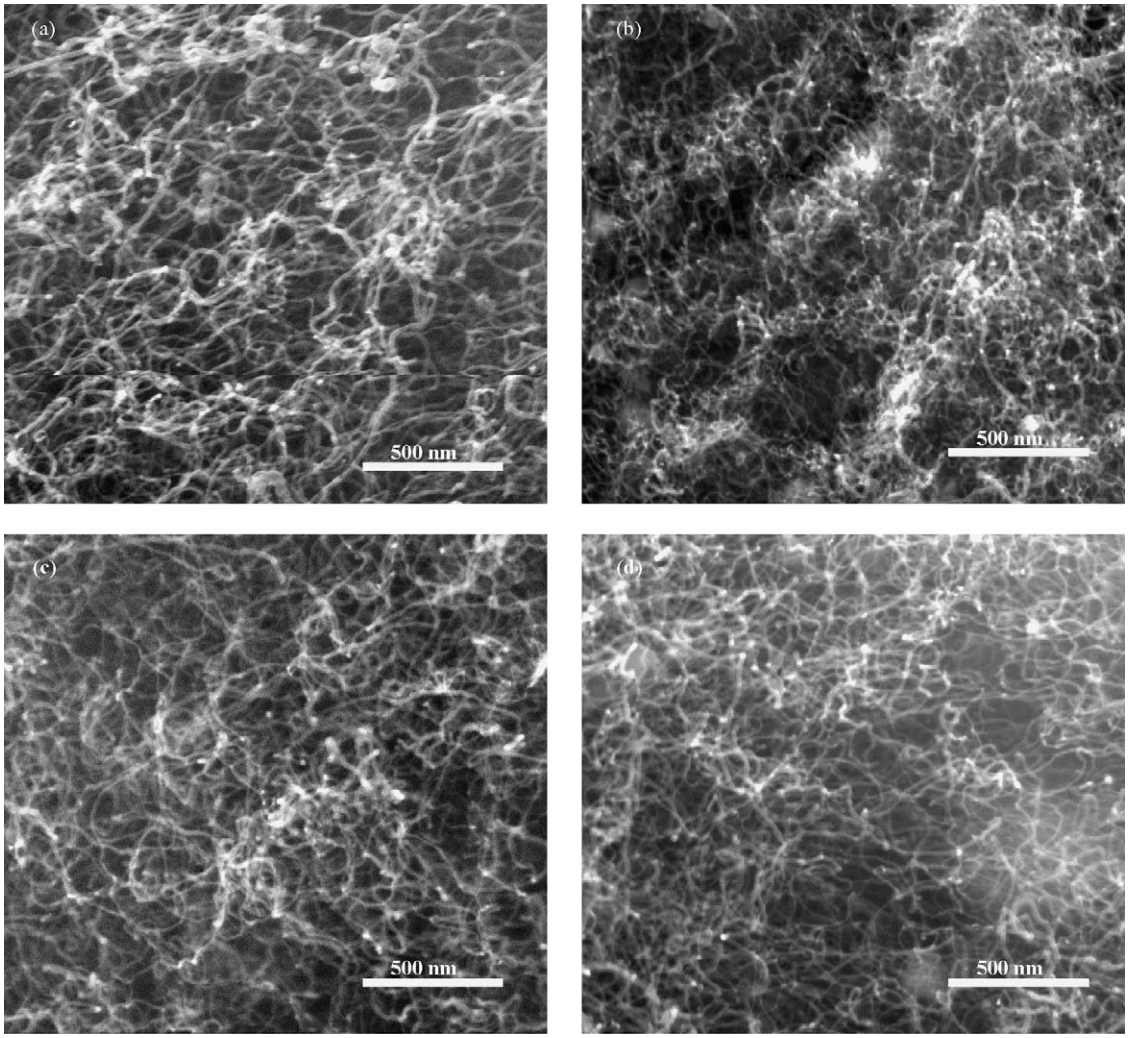

Fig. 11. SEM images of MWCNTs formed by ethanol decomposition over Ni/Al_2O_3 catalysts with different Ni loadings: (a) 50, (b) 70, (c) 80, and (d) 90 mol% at 600 °C.

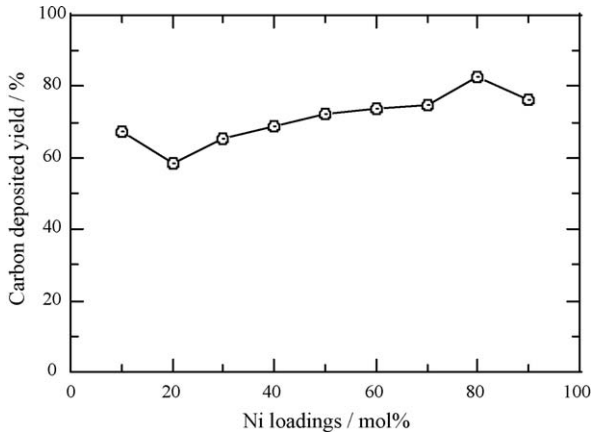

Fig. 12. Changes of the deposited carbon yield as a function of Ni loadings in ethanol decomposition over Ni/Al_2O_3 catalysts at 600 °C.

ethanol decomposition over the Ni (90 mol%)/Al_2O_3 catalyst at 500 °C. Fig. 13 shows the SEM image of CNFs and MWCNTs. It can be found that the diameters of CNFs ranged from 100 to 150 nm. The MWCNTs, with the diameter of 20 nm and the length of a few micrometers, aggregated together and displayed a curled shape. The formation of CNFs and MWCNTs at the same time is a very rare case in the catalytic decomposition of ethanol reported so far. Cabero et al. [35] reported the similar result by catalytic decomposition of acetylene over Fe/silica catalysts under different reaction conditions. They thought that the selectivity of CNF or MWCNT formation depended on the size of metal particles in the catalysts. The smaller metal particles favor the CNT growth, whereas the larger metal particles favor the CNF formation. So, the result in Fig. 13 implies that there might be two different sizes of Ni metal particles in the Ni (90 mol%)/Al_2O_3 catalyst at 500 °C, which resulted in the formation of CNFs and MWCNTs at the same time.

In order to further confirm the presence of two different sizes of Ni particles on the Ni (90 mol%)/Al_2O_3 catalyst, the morphology of deposited products by ethanol decomposition on the catalysts with different Ni loadings at 500 °C was investigated by SEM/BEI techniques. Fig. 14(a)–(c) and (a′)–(c′) shows the SEM images and

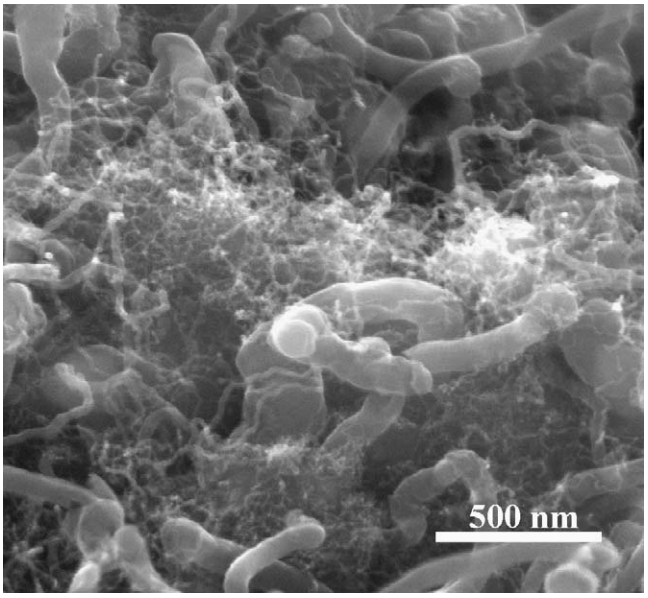

Fig. 13. SEM image of CNFs and MWCNTs formed by ethanol decomposition over Ni (90 mol%)/Al_2O_3 catalyst at 500 °C.

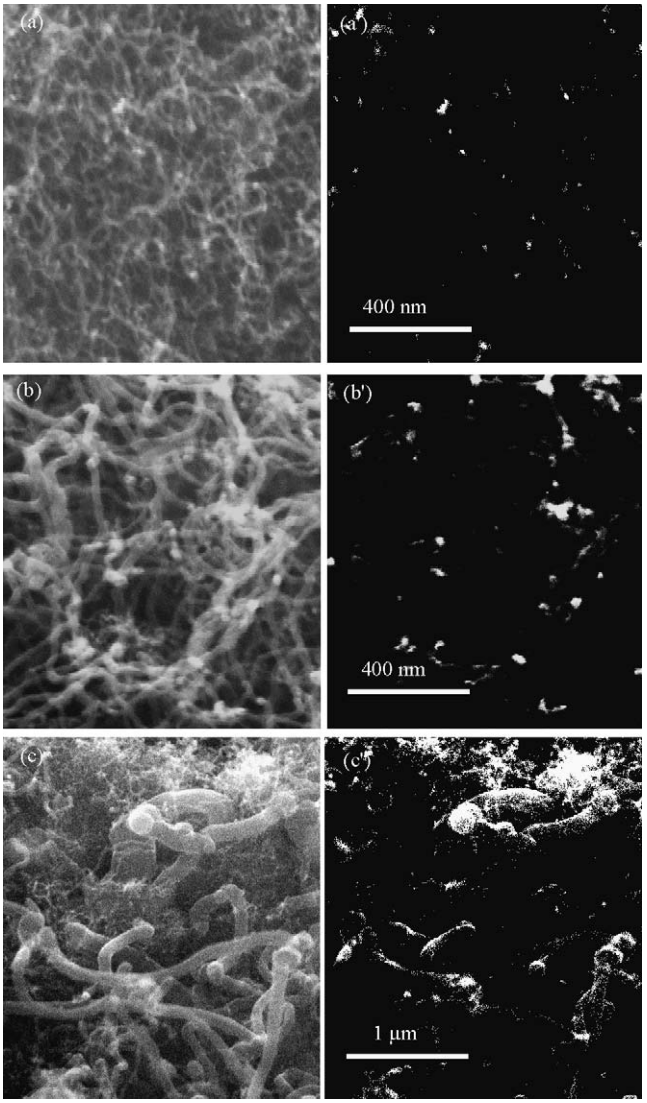

Fig. 14. SEM and back-scattering electron images of deposited products on Ni/Al_2O_3 catalysts at 500 °C; Ni loadings = (a–a') 50, (b–b') 70 and (c–c') 90 mol%.

BEIs of deposited products on the catalysts with Ni loadings of 50, 70 and 90 mol%, respectively. The BEIs were measured at the same time as the corresponding SEM images. All the bright spots in each BEI, which indicate the position and size of Ni metal particles in this case, could be found in the corresponding SEM image at the tips of carbon nanotubes or nanofibers. The SEM images in Fig. 14(a) and (b) indicated the formation of MWCNTs on the Ni(50 and 70 mol%)/Al_2O_3 catalysts, Fig. 14(c) showed the presence of CNFs and MWCNTs on the Ni(90 mol%)/Al_2O_3 catalyst. It is evident from Fig. 14 that the size of Ni metal particles controlling the diameter of carbon nanotubes (or nanofibers) became large with the amount of Ni loading. The increase in the size of Ni particles is due to agglomeration or sintering of the catalyst particles as the Ni loading was increased. On the other hand, two different sizes of Ni metal particles were found to exist in the Ni (90 mol%)/Al_2O_3 catalyst (see Fig. 14(c′)), which led to the formation of CNFs and MWCNTs. However, the similar results over the catalysts with the same Ni loading at 600 °C were not observed in Fig. 11(a)–(d). Accordingly, we think that the selectivity of CNF or MWCNT formation is closely related to not only the amount of Ni loading but also the temperature of reaction. Therefore, the effect of the reaction temperature on the variation of size of Ni particles in the

Table 1
Thermodynamic parameters of the reactions for ethanol decomposition at different temperatures (ΔH^{θ}, ΔG^{θ}: kJ mol^{-1}).

No.	Equations of ethanol decomposition	ΔH^{θ}				ΔG^{θ}			
		500 °C	600 °C	700 °C	800 °C	500 °C	600 °C	700 °C	800 °C
1	$CH_3CH_2OH(g) \rightarrow CO(g) + H_2(g) + CH_4(g)$	53.65	53.24	52.71	52.09	−134.00	−158.25	−182.44	−206.58
2	$CH_3CH_2OH(g) \rightarrow CH_2{=}CH_2(g) + H_2O(g)$	46.05	45.38	44.68	43.97	−52.88	−65.63	−78.31	−90.91
3	$CH_4(g) \rightarrow C(s) + 2H_2(g)$	86.45	87.97	89.17	90.09	5.11	−5.51	−16.28	−27.16
4	$CH_2{=}CH_2(g) \rightarrow 2C(s) + 2H_2(g)$	−41.26	−39.77	−38.57	−37.65	−100.92	−108.74	−116.70	−124.78
5	$2CO(g) \rightarrow C(s) + CO_2(g)$	−172.42	−171.60	−170.70	−169.76	−35.27	−17.58	0.01	17.51
6	$C + H_2O(g) \rightarrow CO(g) + 3H_2(g)$	135.31	135.60	135.77	135.86	24.91	10.61	−3.71	−18.05
7	$CH_4(g) + H_2O(g) \rightarrow CO(g) + 3H_2(g)$	221.76	223.56	224.94	225.94	30.02	5.11	−19.99	−45.21
8	$H_2O(g) + CO(g) \rightarrow H_2(g) + CO_2(g)$	−37.11	−36.00	−34.93	−33.91	−10.36	−6.97	−3.70	−0.54

various Ni loading catalysts, i.e., the selectivity of CNF or MWCNT formation needs further investigation. It will be discussed in our next report.

3.6. A preliminary study on the reactions of ethanol decomposition

In addition to carbon deposition (including nanotubes) on the catalyst and a high yield of hydrogen formation in tail gas, also a few percent of CO and an insignificantly small percent of CH_4 and CO_2 was formed from ethanol decomposition over the Ni/Al_2O_3 catalysts in the range of 500–800 °C. But C_2H_4 was not detected from tail gas tested in this work. The order of fraction of various gas in tail gas was $H_2 > CO > CH_4 > CO_2$, of which the amount of H_2 and CO mainly increased with the temperature rising, and in contrast, CO_2 and CH_4 decreased with temperature. Based on the results, the following reactions and the corresponding standard thermodynamic parameters (ΔH^{θ} and ΔG^{θ}) [36] listed in Table 1 probably better describe the processes of ethanol decomposition at different temperatures:

$$CH_3CH_2OH(g) \rightarrow CO(g) + H_2(g) + CH_4(g) \quad (1)$$

$$CH_3CH_2OH(g) \rightarrow CH_2{=}CH_2(g) + H_2O(g) \quad (2)$$

$$CH_4(g) \rightarrow C(s) + 2H_2(g) \quad (3)$$

$$CH_2{=}CH_2(g) \rightarrow 2C(s) + 2H_2(g) \quad (4)$$

$$2CO(g) \rightarrow C(s) + CO_2(g) \quad (5)$$

$$C(s) + H_2O(g) \rightarrow CO(g) + 3H_2(g) \quad (6)$$

$$CH_4(g) + H_2O(g) \rightarrow CO(g) + 3H_2(g) \quad (7)$$

$$H_2O(g) + CO(g) \rightarrow H_2(g) + CO_2(g) \quad (8)$$

From the viewpoint of thermodynamics equilibrium, the data listed in Table 1 show that the values of ΔG^{θ} for Res. (1), (2), (3), (4), (6) and (7), influenced by the entropy change, decrease gradually with the temperature rising, i.e., the reaction equilibrium constant increased with temperature, revealing that higher temperatures are favorable to these reactions. Res. (5) and (8) are thermodynamically unfavorable at higher temperatures due to the value of ΔG^{θ} increasing with temperature.

Res. (1), (3), (4), (6) and (7) are the reactions of H_2 production, of which (1), (6) and (7) also are the reactions to form CO. As mentioned above, all of them are thermodynamically favorable, so the high temperature favors the production of H_2 and CO. This may be just about the reason why the amount of H_2 and CO increased with the temperature rising. In terms of the carbon production, Res. (3) and (4) may form MWCNTs due to existing Ni active metal site. Comparing with ΔG^{θ} of Res. (3) and (4), it concludes that the reaction of further decomposing C_2H_4 to produce H_2 and C more easily take place than that of further decomposing CH_4 because ΔG^{θ} of Re. (4) is much smaller (or much more negative) than that of Re. (3) at any temperature. This may explain the reason why there is no C_2H_4 detected in tail gas but the presence of CH_4. Similarly, Res. (3) and (7) as the thermodynamically favored reactions may explain the reason why CH_4 in tail gas decreased with increasing temperature. While Res. (5) and (8) to form CO_2 as the thermodynamically unfavorable reactions also indicate the reason why the amount of CO_2 decreased with the temperature increase.

4. Conclusion

The decomposition of ethanol over Ni/Al_2O_3 catalysts with different Ni loadings was investigated in the temperature range of 500–800 °C. The influence of the temperature and the loading amounts of Ni/Al_2O_3 catalysts on the hydrogen production and the MWCNT growth was discussed systematically. A concept of simultaneous production of hydrogen and MWCNTs from ethanol decomposition was suggested. Several possible reactions for ethanol decomposition to produce hydrogen and carbon (including nanotube) and so on at the same time were also proposed. The optimal experimental conditions for the production of hydrogen and for the growth of MWCNTs were proposed. The higher temperature (700 or 800 °C) favored the hydrogen production over the catalysts with the high Ni loadings (50–90 mol%) based on the ethanol conversion and the H_2 yield, but resulted in the reduction of the amount of MWCNTs. The Ni (80 mol%)/Al_2O_3 was the most effective catalyst for the production of hydrogen and the growth of MWCNT by ethanol decomposition at 600 °C. A method is presented with which it is possible for ethanol decomposition to grow MWCNTs and CNFs simultaneously over the Ni (90 mol%)/Al_2O_3 at 500 °C. This may be because there were two different sizes of Ni metal particles in the catalyst. In addition, a preliminary investigation on ethanol decomposition to produce hydrogen and carbon was proceeded and the possible reactions occurred during ethanol decomposition were suggested.

Acknowledgements

The authors acknowledge the financial supports of the National Hi-Tech Research and Development Program (863) of China (No. 2007AA05Z116), the National Natural Science Foundation of China (Nos. 20673082 and 20873099), the scientific research foundation for ROCS, SEM. (No. 2006331), the key project of science and technology of Shaanxi Province (No. 2005k07-G2), and the natural science foundation of Shaanxi education Committee (No. 06JK167). The authors are also grateful to the State Key Laboratory of Continental Dynamics for the SEM measurements.

References

[1] J.D. Holladay, Y. Wang, E. Jones, Chem. Rev. 104 (2004) 4767.
[2] P.Y. Sheng, A. Yee, G.A. Bowmaker, H. Idriss, J. Catal. 208 (2002) 393.
[3] T. Davidian, N. Guilhaume, E. Iojoiu, H. Provendier, C. Mirodatos, Appl. Catal. B 73 (2007) 116.
[4] S. Takenaka, S. Kobayashi, H. Ogihara, K. Otsuka, J. Catal. 217 (2003) 79.
[5] W. Qian, T. Liu, Z. Wang, F. Wei, Z. Li, G. Luo, Y. Li, Appl. Catal. A 260 (2004) 223.
[6] S.H.S. Zein, A.R. Mohamed, Energy Fuels 18 (2004) 1336.
[7] S. Takenaka, M. Serizawa, K. Otsuka, J. Catal. 222 (2004) 520.
[8] Y. Wang, N. Shah, G.P. Huffman, Catal. Today 99 (2005) 359.
[9] R.M. Almeida, H.V. Fajardo, D.Z. Mezalira, G.B. Nuernberg, L.K. Noda, L.F.D. Probst, N.L.V. Carreno, J. Mol. Catal. 259 (2006) 328.
[10] A. Birot, F. Epron, C. Descorme, D. Duprez, Appl. Catal. B 79 (2008) 17.
[11] T. Montini, L.D. Rogatis, V. Gombac, P. Fornasiero, M. Graziani, Appl. Catal. B 71 (2007) 125.
[12] Y.Z. Yang, C.-H. Chang, H. Idriss, Appl. Catal. B 67 (2006) 217.
[13] G.B. Sun, K. Hidajat, X.S. Wu, S. Kawi, Appl. Catal. B 81 (2008) 303.
[14] J.L. Davis, M.A. Barteau, Surf. Sci. 187 (1987) 387.
[15] N. Laosiripojana, W. Sutthisripok, S. Assabumrungrat, Chem. Eng. J. 127 (2007) 31.
[16] R. Barthos, A. Széchenyi, Á. Koós, F. Solymosi, Appl. Catal. A 327 (2007) 95.
[17] R.H. Baughman, A.A. Zakhidov, W.A. Heer, Science 297 (2002) 787.
[18] A. Thess, R. Lee, P. Nikolaev, H. Dai, P. Petit, J. Robert, C. Xu, Y.H. Lee, S.G. Kim, A.G. Rinzler, D.T. Colbert, G.E. Scuseria, D. Tomanek, J.E. Fischer, R.E. Smalley, Science 273 (1996) 483.
[19] C. Journet, W.K. Maser, P. Bernier, A. Loiseau, M.L. Chapelle, S. Lefrant, Nature 388 (1997) 756.
[20] R.G. Ding, G.Q. Lu, Z.F. Yan, M.A. Wilson, J. Nanosci. Nanotech. 1 (2001) 7.
[21] S. Noda, H. Sugime, T. Osawa, Y. Tsuji, S. Chiashi, Y. Murakami, S. Maruyama, Carbon 44 (2006) 1414.
[22] M. Hu, Y. Murakami, M. Ogura, S. Maruyama, T. Okubo, J. Catal. 225 (2004) 230.
[23] L. Huang, X. Cui, B. White, S.P. O'Brien, J. Phys. Chem. B 108 (2004) 16451.
[24] A. Grüneis, M.H. Rümmeli, C. Kramberger, A. Barreiro, T. Pichler, R. Pfeiffer, H. Kuzmany, T. Gemming, B. Büchner, Carbon 44 (2006) 3177.
[25] L.A. Montoro, P. Corio, J.M. Rosolen, Carbon 45 (2007) 1234.
[26] Y.L. Li, I.A. Kinloch, A.H. Windle, Science 304 (2004) 276.
[27] N. Laosiripojana, S. Assabumrungrat, Appl. Catal. B 66 (2006) 29.
[28] W.L. Li, H. Wang, Z.Y. Ren, G. Wang, J.B. Bai, Appl. Catal. B 84 (2008) 433.
[29] K. Kakehi, S. Noda, S. Chiashi, S. Maruyama, Chem. Phys. Lett. 428 (2006) 381.
[30] K. Bartsch, B. Arnold, R. Kaltofen, C. Täschner, J. Thomas, A. Leonhardt, Carbon 45 (2007) 543.
[31] W. Li, H. Zhang, C. Wang, Y. Zhang, L. Xu, K. Zhu, S. Xie, Appl. Phys. Lett. 70 (1997) 2684.
[32] P. Ramesh, N. Kishi, T. Sugai, H. Shinohara, J. Phys. Chem. B 110 (2006) 130.
[33] W. Qian, T. Liu, Z. Wang, H. Yu, Z. Li, F. Wei, G. Luo, Carbon 41 (2003) 2487.
[34] M. Glerup, H. Kanzow, R. Almairac, M. Castignolles, P. Bernier, Chem. Phys. Lett. 377 (2003) 293.
[35] M.P. Cabero, I.R. Ramos, A.G. Ruíz, J. Catal. 215 (2003) 305.
[36] X.C. Fu, W.X. Shen, T.Y. Yao, Physical Chemistry, second ed., High Education Press, Beijing, 2000.